ASCE

Macromodeling Approach and Robustness Enhancement Strategies for Steel Frame Buildings with Composite Slabs against Column Loss

Junjie Wang[1] and Wei Wang, M.ASCE[2]

Abstract: This study presents a numerical assessment of the behavior of seismically designed steel frame buildings against ground floor column loss. In the designed prototype buildings, moment frames with beam-to-column rigid connections and concentric X-bracing frames resist the lateral force, whereas the steel-concrete composite floor slabs resist the gravity load. Macromodels are used to capture the building response when removing ground floor columns. The macromodels are built with a reduced modeling approach, in which the concrete damage and the local steel fracture behavior are accurately considered. The macromodeling approach is calibrated by high-fidelity models and validated by composite floor test. The validated macromodels are used to investigate the effect of column loss location, total number of floors, floor slab, beam-to-column connection type, adjacent span, and steel brace on the collapse resistance of prototype buildings. To account for sudden column failure, an energy-based approach is used to convert the quasi-static response curves to dynamic response curves. The structural robustness is derived by comparing each column failure case's dynamic ultimate capacities with corresponding design requirements. Structural robustness enhancement strategies for steel frame buildings under progressive collapse scenarios are summarized and discussed. Moreover, a retrofitted moment-resisting connection with steel strands is proposed to enhance the steel frame buildings' robustness by providing a second line of defense. **DOI: 10.1061/(ASCE)ST.1943-541X.0003214.**

Author keywords: Disproportionate collapse; Progressive collapse; Steel buildings; Composite slab; Membrane action; Macromodel.

Introduction

Progressive collapse of structure is the phenomenon by which initial local component failure can successively spread to surrounding components, eventually resulting in devastating consequences, such as the collapse of an entire structure or a disproportionately large part of it (Starossek 2009). Several current guidelines (CEN 2006; GSA 2016; DoD 2016) addressing progressive collapse require that structural robustness must be sufficient to prevent disproportionate collapse. Starossek and Haberland (2011) defined the term "structural robustness" as the "insensitivity of a structure to local failure," whereas a broader definition is given in European Committee for Standardization (CEN 2006): "the ability of a structure to withstand abnormal events without being damaged to an extent disproportionate to the original cause." The difference between these two definitions is whether or not the triggering events of local failure are taken into account. The definition proposed by Starossek and Haberland (2011) is threat independent, more pragmatic, and more widely accepted (CNPI 2011; ASCE 2017; Khandelwal and El-Tawil 2011; Bao et al. 2017).

The definition of structural robustness is comprehensible but still controversial and challenging to quantify. Robustness is a property involving many structural indicators, such as redundancy, ductility, vulnerability, exposure, and others. ASCE/SEI 7-16 (ASCE 2017) proposes that structural robustness can be evaluated by "notional removal of key load-bearing structural elements, followed by a structural analysis to assess the ability of the structure to bridge over the damage." Starossek and Haberland (2011) proposed three quantitative measures, including stiffness-based measure, damage-based measure, and energy-based measure, for quantifying structural robustness. Even though these measures are expressive and general, they are impracticable and difficult to calculate for complicated structures. Izzuddin et al. (2008), Khandelwal and El-Tawil (2011), Main (2014), and Bao et al. (2017) proposed a practical capacity-based measure, which is based on the ultimate capacity of the target structure under single column loss scenarios. Nonlinear static pushdown analysis (Main 2014; Bao et al. 2017) or nonlinear incremental dynamic analysis (Khandelwal and El-Tawil 2011) can be used to compute the ultimate capacity after column failure. To capture the structural response after sudden column loss, the nonlinear incremental dynamic analysis is the most accurate option but needs to run multiple dynamic analyses with incrementally increasing gravity load to capture the ultimate capacity (Khandelwal and El-Tawil 2011). Based on energy conservation, the static responses obtained from the nonlinear static pushdown analysis are converted into equivalent dynamic responses (Main 2014; Bao et al. 2017). Compared with the nonlinear incremental dynamic analysis, the nonlinear static pushdown analysis needs only to perform a single analysis. As a result, the computing cost is significantly decreased with this method.

Therefore, a similar method as Bao et al. (2017) is utilized in this study. The target structures subjected to different ground floor column loss are simulated using the nonlinear static pushdown analyses, and the obtained static responses are converted into corresponding equivalent dynamic responses. Considering all of the column failure scenarios, the minimum ratio between the ultimate dynamic capacity and the corresponding applied gravity load is

[1]Graduate Student, Dept. of Structural Engineering, Tongji Univ., Shanghai 200092, China. Email: ruida91@outlook.com

[2]Professor, State Key Laboratory of Disaster Reduction in Civil Engineering, Dept. of Structural Engineering, Tongji Univ., Shanghai 200092, China (corresponding author). ORCID: https://orcid.org/0000-0003-1241-465X. Email: weiwang@tongji.edu.cn

Note. This manuscript was submitted on August 20, 2020; approved on August 11, 2021; published online on October 23, 2021. Discussion period open until March 23, 2022; separate discussions must be submitted for individual papers. This paper is part of the ***Journal of Structural Engineering***, © ASCE, ISSN 0733-9445.

selected as the robustness index. If the robustness index is greater than unity, the structure is robust enough to prevent progressive collapse under all column failure scenarios; otherwise, suitable strategies and measures must be taken to enhance the structural robustness.

As noted by Alashker et al. (2011), planar analysis is not reliable for the progressive collapse simulation, and full three-dimensional (3D) analysis is the only accurate way to strictly investigate the structural robustness of an entire building. Apart from this, the floor slab can significantly improve the robustness of the structure, and its influence must be considered (Sadek et al. 2008; Alashker et al. 2010; Li and El-Tawil 2014; Johnson et al. 2016; Hadjioannou et al. 2018). The entire steel frame building analyses are time-consuming and require high computational cost. Hence, macromodels are usually selected to replace high-fidelity models to reduce the computational time (Fu 2009, 2010; Kwasniewski 2010; Alashker et al. 2011; Li and El-Tawil 2014). As noted by Wang et al. (2019b), the local stress state, including stress triaxiality and Lode angle, must be taken into account when simulating the progressive collapse of steel structures. But, in the macromodel, reflecting the influence of the local stress state on the steel fracture at the connection region is challenging. Up to now, this problem has not been satisfactorily solved. To settle this matter, this study presents a modeling approach for the macromodel of steel frame buildings, and the corresponding modeling methodology is illustrated in Fig. 1. High-fidelity models are calibrated and validated based on the test results of a full-scale composite floor test and related coupon tests (Wang et al. 2019b). Then, the high-fidelity models are used to calibrate the macromodel, and the calibrated macromodel is verified by comparing its results with the composite floor test. Subsequently, this modeling approach is applied to the progressive collapse simulation of a specially designed five-story prototype building. Based on this building, the influence of some key factors, including column failure location, total number of floors, floor slab, beam-to-column connection type, adjacent span, and steel brace, on the collapse resistance are investigated.

Next, the structural robustness of the prototype building is assessed. Meanwhile, a retrofitted moment-resisting connection with steel strands is proposed and applied to the prototype building. The effectiveness of this developed connection in enhancing structural robustness is validated. Additionally, structural robustness enhancement strategies for steel frame buildings under progressive collapse scenarios are summarized and discussed.

Composite Floor Test

As previously mentioned, the macromodel of the composite floor is calibrated using the high-fidelity model, which is calibrated and validated by a full-scale composite floor test (Wang et al. 2020). In this test, a middle-edge column removal scenario is investigated. Fig. 2(a) depicts the plan view of the test specimen. The member dimensions are H200 (section height) × 100 (flange width) × 5.5 (web thickness) × 8 (flange thickness) for girders, H150 × 75 × 7 × 10 for beams, and H200 × 200 × 8 × 12 for columns, respectively. Except for the removed column, all column bases are

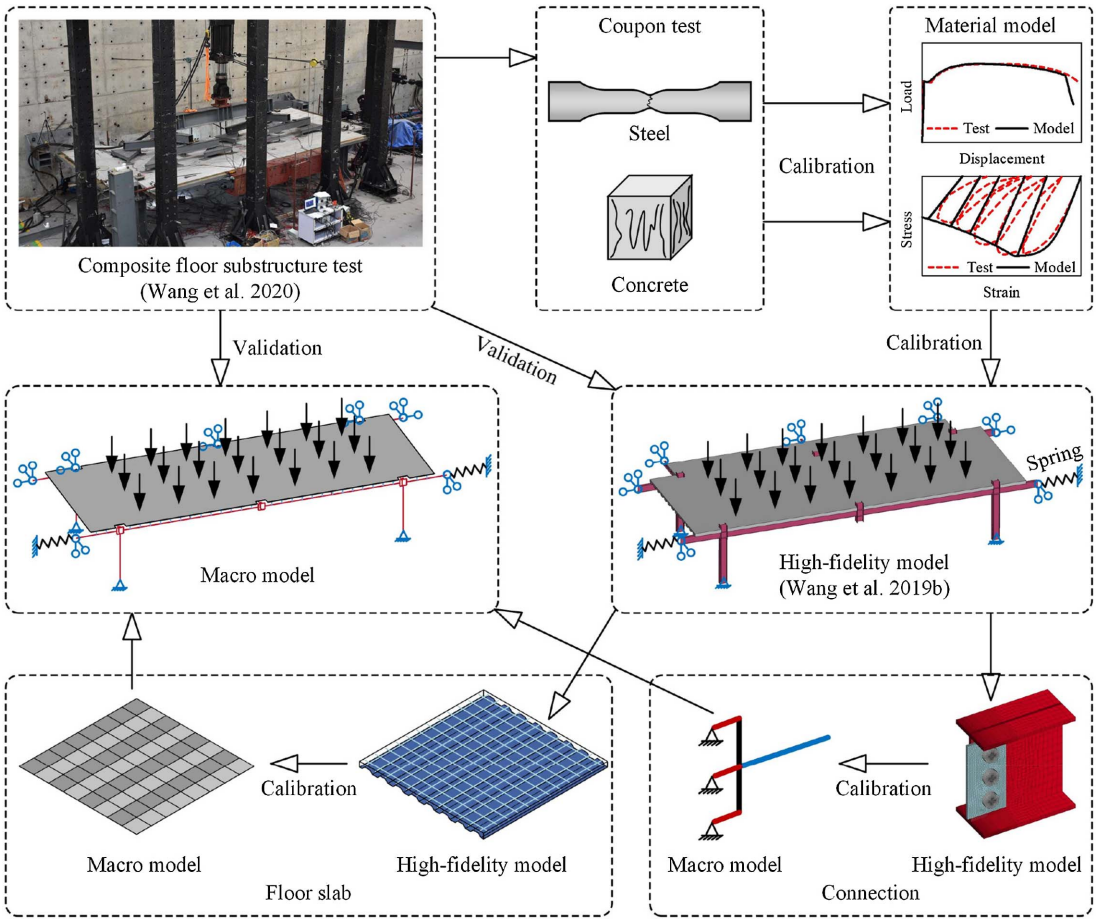

Fig. 1. Modeling methodology flowchart.

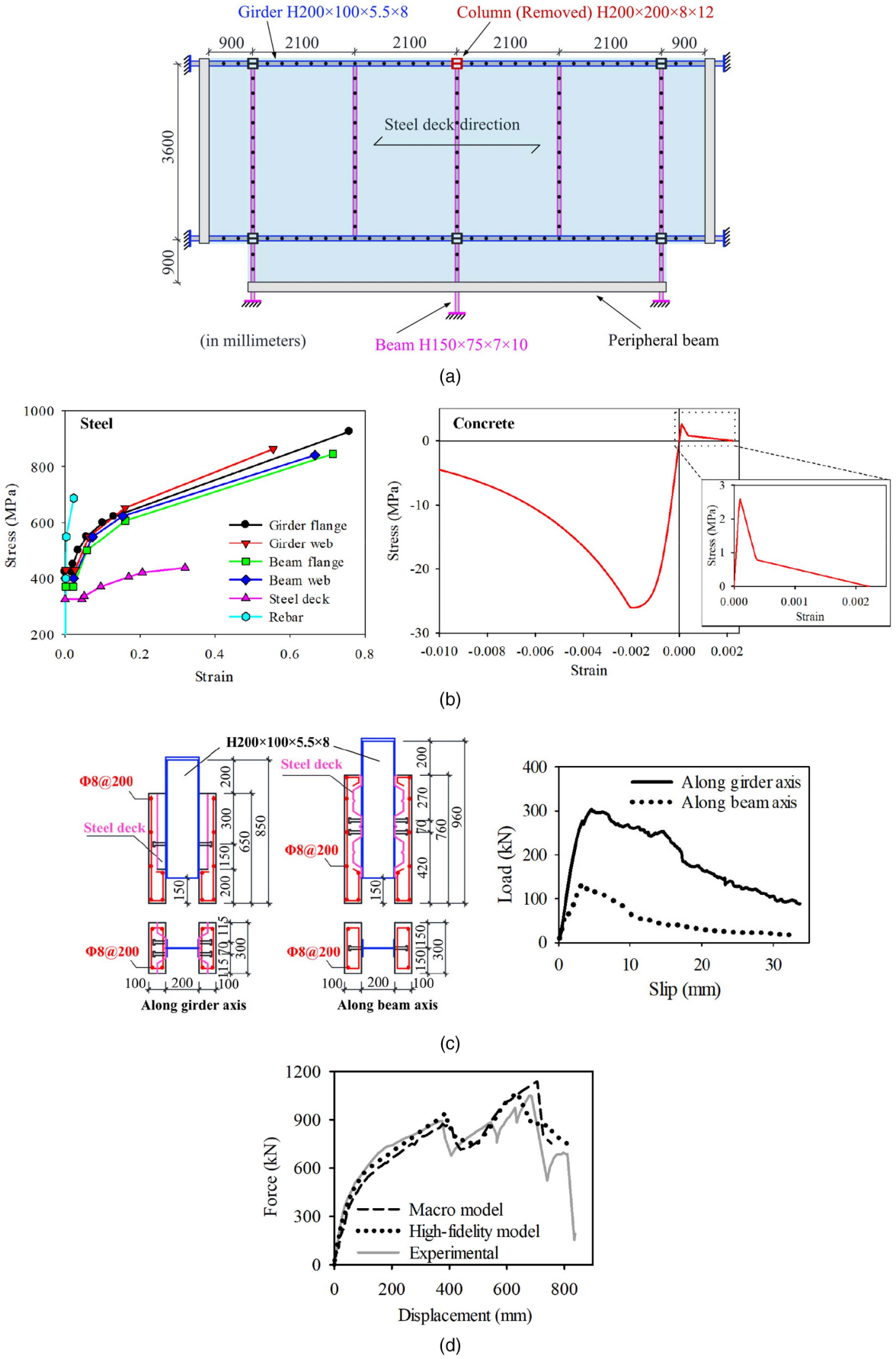

Fig. 2. Composite floor test.

fixed during the test. The girders are connected to the columns with a welded flange-bolted web (WFBW) connection. The beams are connected to the girders and columns with a shear tab connection. The total thickness of the composite slab used in this specimen is 100 mm. The corrugation depth of the 1.2 mm trapezoidal steel deck is 50 mm, and the thickness of the slab flange is 50 mm. The ribs of the steel decks are oriented parallel to the girder line. The concrete slab is reinforced by steel meshes with 8-mm diameter rebars at 200-mm spacing. Composite action between beams and composite slabs are achieved through 16 mm-diameter shear studs at 300- and 305-mm spacing along the girder and beam directions, respectively. Push-out tests are conducted to determine the load-slip behavior of the shear studs along the girder and beam directions, as indicated in Fig. 2(b). To simulate the boundary constraints of the surrounding bays, 900 mm extra slabs are extended at the horizontal boundaries. Moreover, the extended floor beams are also constrained at their ends by horizontal supports. During the test, a significant catenary force is developed in the girders connected to the removed column and causes lateral movements that cannot be ignored at their ends. By diving the measured lateral force and lateral displacement, the horizontal elastic stiffness of the horizontal supports at these locations is approximately equal to 10 kN/m (Wang et al. 2019b, 2020). In the test, a displacement-controlled vertical load of the actuator is uniformly distributed to 24 points on the specimen's slab to simulate the uniform gravity load. The principal material properties of the steel used in this specimen are indicated in Fig. 1(c). The cylindrical compressive strength of concrete is 26 MPa. More details for this test can be found in Wang et al. (2020).

High-Fidelity Model of Composite Floor

A high-fidelity model (Fig. 1) is built based on the composite floor test and is described in detail by Wang et al. (2019b), and the modeling scheme is briefly presented here. Steel members, including girders, beams, columns, and steel decks, are modeled by shell elements. Truss and beam elements are used to model rebars and shear studs, respectively. Reduced-integration solid elements are used to model the concrete slab. The nonlinear material behaviors, including ductile fracture of steel and plastic damage of concrete, are accurately calibrated based on the coupon test results. Nonlinear spring elements are used to model the load-slip relationship between shear studs and floor beams, and their load-slip relationships are derived from the push-out tests. The element nodes of rebar and shear stud are merged with their surrounding concrete elements to enforce a perfect bond between them. Spring elements are used to simulate the lateral restraint stiffness at the girder ends that are colinear with the removed column. Other deformations at the ends of the extended floor beams are fully restrained. The floor load applied by the test setup is simulated by applying a uniform vertical load to the floor region affected by the removed column. The accuracy of the high-fidelity model has been validated by Wang et al. (2019b), and the load-displacement relationships of this model and the test are compared in Fig. 2(d). In the next section, this high-fidelity modeling method is used to calibrate the macromodel of the composite floor.

Macromodeling Approach of Composite Floor

This section presents a macromodel of the aforementioned composite floor test, which is implemented using the LS-DYNA version R11.0 software.

Girder-to-Column Connection

Fig. 2(a) indicates the macromodel of the composite floor in the vicinity of the girder-to-column connection. Hughes-Liu beam elements are used to model the girders, beams, and columns. The spring elements are used to model the welded girder flanges and bolted shear tab connections. The nonlinear behavior of these spring elements is modeled using a general spring material model, which is the No. 119 material in LS-DYNA. As indicated in Fig. 3(b), the axial load-deformation relationships of these spring elements are represented by a trilinear model, similar to that proposed by Sadek et al. (2008). After the ultimate tensile resistance (t_u) is reached, the trilinear model decreases linearly until it becomes zero at the fracture displacement (δ_0). The axial resistance remains unchanged after the ultimate compressive resistance ($-t_u$) is reached. In the test, the girder-to-column and beam-to-column connections were all failed by tension failure, whereas shear and out-of-plane failures were not observed. Hence, the spring deformations along these directions are rigidly constrained. A similar procedure is also used by Sadek et al. (2008), Yang and Tan (2013), and Ding et al. (2017).

The fracture performance of the girder-to-column connections under progressive collapse scenarios is highly affected by the stress state parameters, including stress triaxiality and lode angle. Ductile fracture models, incorporating the effects of stress triaxiality and lode angle, were determined by steel coupons extracted from the composite floor specimen (Wang et al. 2019b). However, these fracture models cannot be applied directly to the beam elements because the local stress state cannot be accurately determined by the beam element. To overcome this difficulty, an indirect method is employed: a high-fidelity model is built to simulate the fracture behavior of the girder-to-column connection, and its results are used to calibrate the corresponding macromodel. The detailed calibration procedure is illustrated in Fig. 2(c). The web spring is first calibrated using a bolted shear tab connection model extracted from the girder-to-column connection. Both bolted shear tab connections built by the high-fidelity and macromethods are subjected to the monotonic tensile loading along the girder axis. After several adjustments, the web spring parameters are determined when the result of the macromodel matches that of the high-fidelity model. Then, as indicated in Fig. 2(c), the flange spring is calibrated using a half-span girder model that can approximately represent the performance of the girder-to-column connection under the column removal scenario (Wang et al. 2019b). In the half span model, the constraint that comes from the column is simplified to a rigid boundary, whereas a monotonic vertical loading is applied to the horizontally restrained girder end. Both the high-fidelity and macromodels are built for the half-span model. The calibrated web spring is used in this half-span macromodel. Noteworthy is that, for the flange springs, t_y and t_u equal the tensile yield and ultimate capacities of the flange section, whereas δ_y equals the yield deformation of the flange. Therefore, only δ_u and δ_0 need to be calibrated for the flange spring. In a similar manner to that previously described, the flange spring parameters are calibrated when the result of the macromodel fits well with that of the high-fidelity model. Because the bolt connection dimensions and material properties of the beam-to-column connection are identical to those of the girder-to-column connection, the calibrated web spring for the girder-to-column connection is used in the macromodel of the beam-to-column connection. The parameters of the calibrated connection springs are listed in Table 1. Because the high-strength bolts are used, the failure of the bolted shear tab connection is assumed to be induced by the fracture of shear tabs or beam webs rather than the bolt shear failure. Therefore, this modeling method might not be directly applied to the connections governed by the bolt shear failure mode.

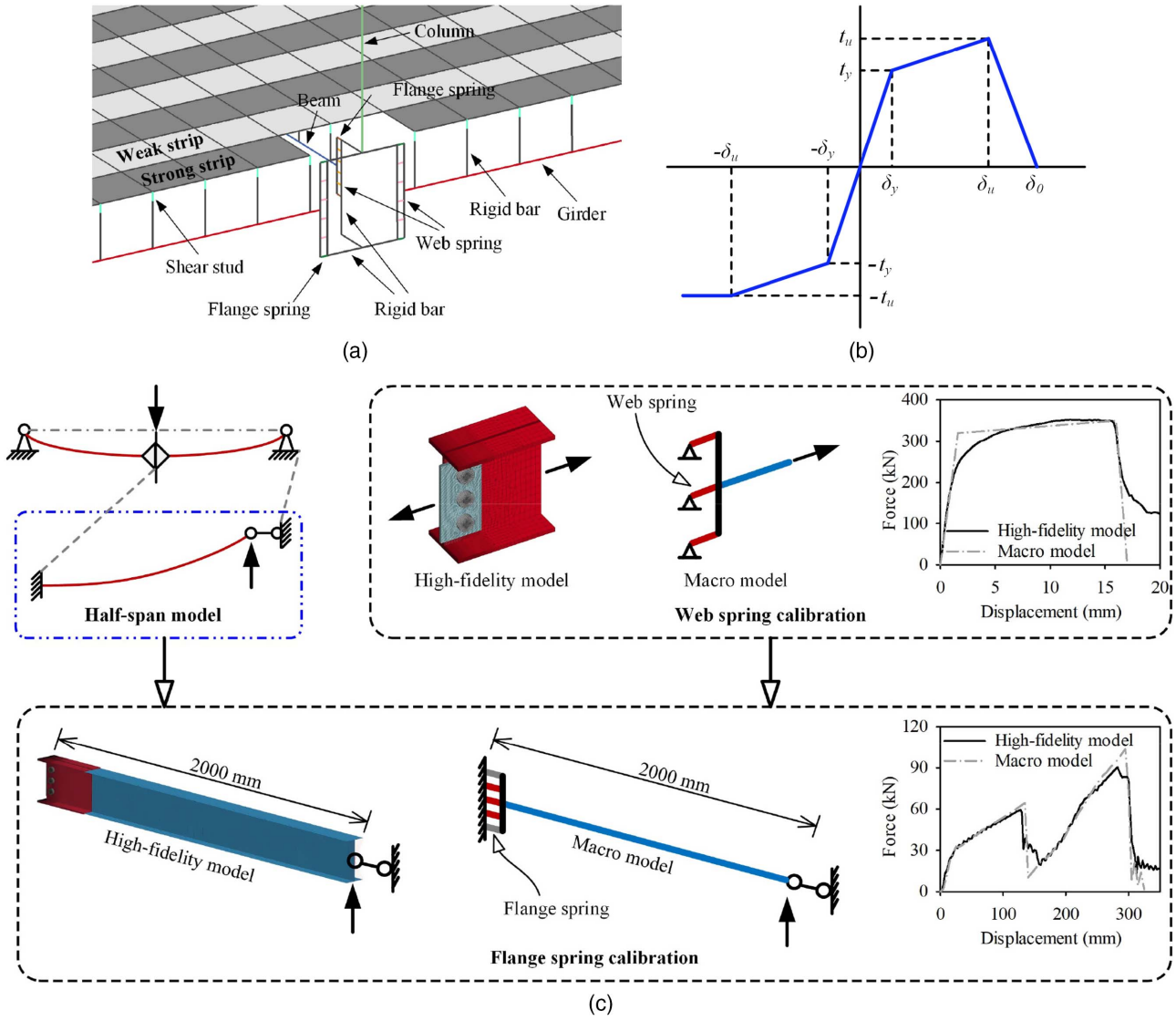

Fig. 3. Macromodeling of girder-to-column connection.

Table 1. Calibrated connection spring parameters

Spring	δ_y (mm)	t_y (kN)	δ_u (mm)	t_u (kN)	δ_0 (mm)
Web spring	1.6	107	16	117	17
Flange spring	0.02	300	1.7	400	2

Composite Floor Slab

Fig. 4(a) illustrates the modeling and calibration approach for the macromodel of the composite slab. To reduce computing time, shell elements with through-thickness integration are used to model the composite slab. Shell elements are divided into two categories (strong strip and weak strip) to reflect the variation in section height of the corrugated composite slab. The 50-mm thick slab flange section is presented by a weak strip, whereas the 100-mm thick slab section with flange and rib is represented by the strong strip. A total of seven integration points are used in the strong strip, including one steel deck point, two rebar points, and four concrete points. Because only the deck ribs are constrained to the floor beams by the shear studs, the steel deck point is not modeled in the weak strip. Hence, the weak strip is composed of two rebar points and four concrete points. To ensure model continuity, the element nodes of the strong strip are defined at the midthickness section of the composite slab, whereas the element nodes of the weak strip are defined at the bottom surface of the slab flange.

The material 172 in LS-DYNA is used to simulate the steel deck, rebar, and concrete in the shell elements. By changing the reinforcement rate, this material model can simulate smeared rebar, plain concrete, or a combination of both. Fig. 2(b) presents the stress-strain curves for different materials used in this material model. Two separate integration points are used to model the rebars in two directions. Hence, the rebar fracture in one direction does not induce the premature failure of rebars in the transverse direction. Limited by the trapezoidal cross-section, the steel deck cannot develop significant tensile force in the direction perpendicular to the deck ribs. Given this behavior, in the steel deck point, the steel deck property is only defined in the direction parallel to the deck ribs. To avoid the convergence problem resulting from a too large unrealistic element distortion, when the plastic strain reaches 0.3, the corresponding shell element is removed from the model.

Under the progressive collapse scenario, the load-carrying capacity of the composite slab is mainly provided by the bending resistance and the tensile membrane action. As indicated in Fig. 4,

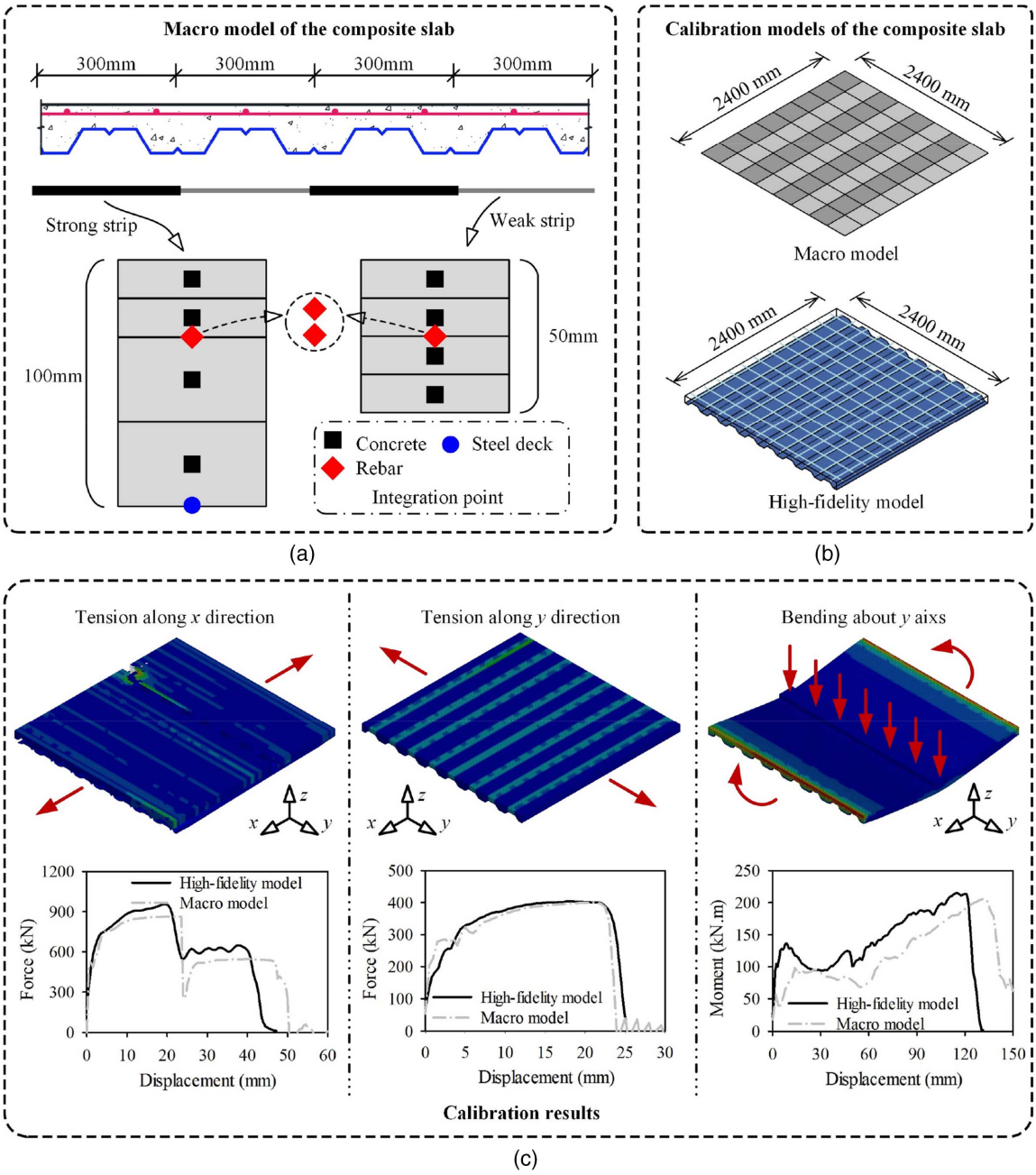

Fig. 4. Macromodeling of composite slab.

limited by the corrugated cross-section, the composite slab used in this study acts as a one-way slab and can only develop bending resistance about the y-axis (perpendicular to the deck ribs). In contrast, tensile forces can be developed along both the x-axis (parallel to the deck ribs) and the y-axis. The tensile forces along the x-axis are developed by steel decks and rebars, whereas the tensile forces along the y-axis are only developed by the rebars. Therefore, as indicated in Fig. 4, the macromodel of the composite slab is calibrated in terms of three loading cases: tension along the x-axis, tension along the y-axis, and bending about the y-axis. The benchmark model for the calibration is a square composite slab extracted from the test specimen, with a size $2{,}400 \times 2{,}400$ mm. Both the high-fidelity and macromodels are built for it. Because only the deck ribs are constrained by the shear studs, for the steel deck in the high-fidelity model, only element nodes at the bottom surfaces are applied with a horizontal constraint (bending about the y-axis) or tensile force (tension along the x-axis). After several adjustments, the macromodel is calibrated when its results match those of the high-fidelity model, and the comparison between them is provided in Fig. 4. The element number of the macromodel and high-fidelity model is 64 and 41,088, respectively. Therefore, the macromodel significantly reduces computational costs.

Shear Stud

As indicated in Fig. 2(c), the load-slip relations and the shear capacity of the shear stud are obtained by conducting push-out tests. In the macromodel of the composite floor (Fig. 3a), rigid bars extend from the element nodes of girders and beams to their top flanges, and the composite slabs are connected to these rigid bars by

discrete beam elements. A general spring material model—material 119 in LS-DYNA—is applied to these discrete beam elements to simulate the shear studs. The spring is defined with the parameters described by Wang et al. (2019b).

Comparison with Experimental Results

In the macromodel of the composite floor (Fig. 1), an incrementally increasing vertical load is uniformly applied to the floor region affected by the removed column until the macromodel loses load-carrying capacity. According to the experimental design, all column bases are fixed except for the removed column. The lateral restraints at the girder ends that are colinear with the removed column are simulated by spring elements with stiffness of 10 kN/mm, as previously mentioned. Other deformations at the ends of the floor beams are fully restrained. The total vertical reaction at the bases of all columns is considered as the floor resistance. The numerically calculated floor resistance versus vertical displacement curve at the removed column is drawn in Fig. 2(b), which matches well with that obtained from the test data. Two principal peak load points, caused by the failure development at the girder-to-column connection, are successfully captured. Hence, this macromodeling approach is adopted in the following section.

Prototype Buildings

Two five-story prototype steel frame buildings, Building A (Fig. 5a) and Building B (Fig. 5b), are designed according to Chinese codes [GB 50017-2017 (MOHURD 2017); GB 50011-2010 (MOHURD 2010)]. The seismic design intensities of Building A and Building B are VI and VIII, respectively. The design basic earthquake accelerations of Building A and Building B are 0.05 and 0.20 g (gravitational acceleration), respectively. Compared with Building A,

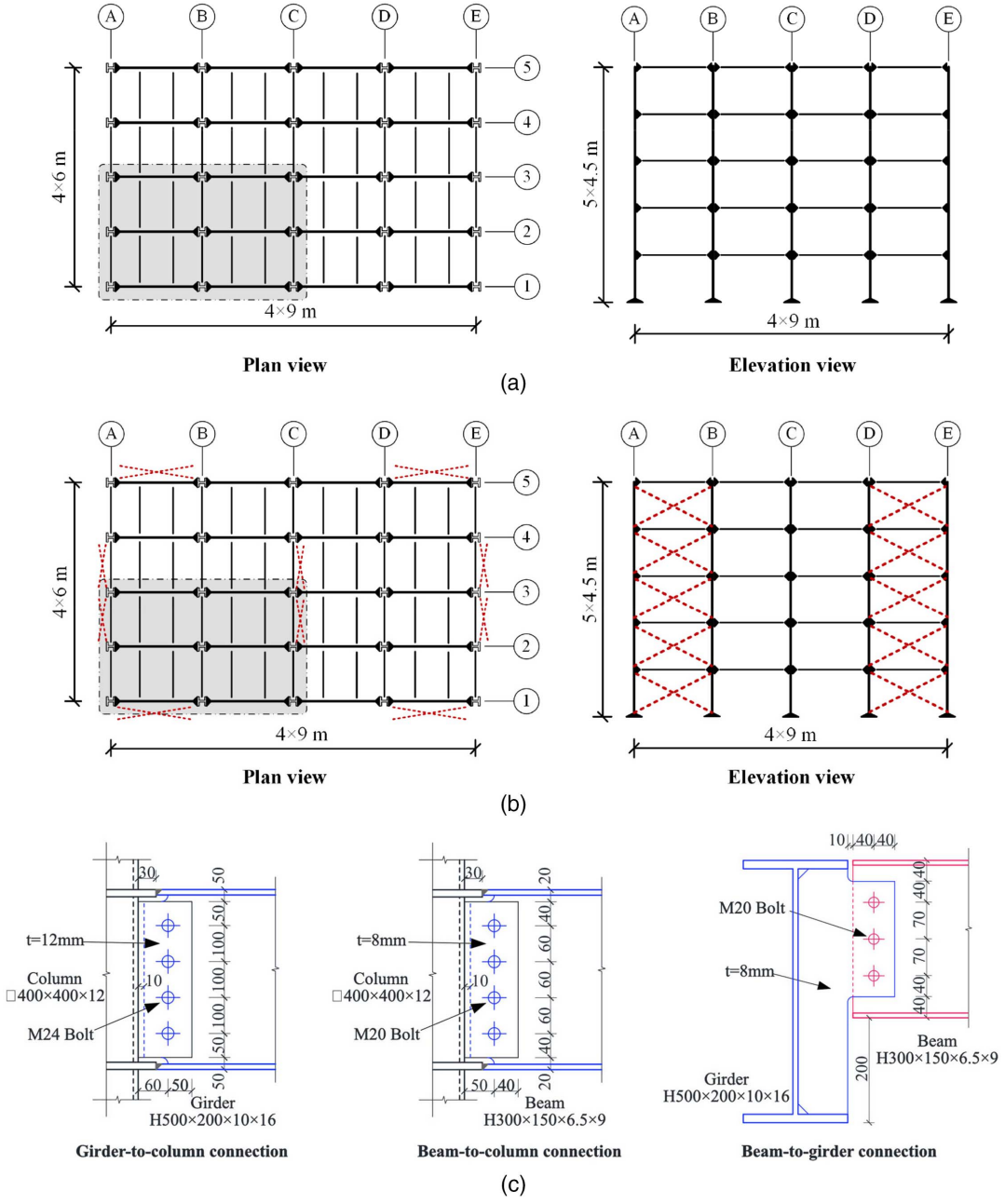

Fig. 5. Prototype buildings.

J. Struct. Eng., 2022, 148(1): 04021238

the excess seismic loads in Building B are resisted by steel braces. Except for the concentric steel braces, all structure dimensions are identical for these two buildings. In these two buildings, the height of each floor is 4.5 m, the girder span is 9 m, the beam span is 6 m, and the beam spacing is 3 m. The design dead load (DL) is 5 kN/m^2, and the live load (LL) is 2 kN/m^2. The composite floor slab is identical to that indicated in Fig. 3(a). The steel deck and slab reinforcement used in the composite slabs are the same as those used by Wang et al. (2020). As indicated in Fig. 5(c), all of the girder-to-column connections and beam-to-column connections are WFBW connections, whereas the beam-to-girder connections are bolted shear tab connections. Square steel tube columns with a section of □400 × 12 are used in these buildings. H-shaped steel girder and beam are used and have section sizes of H500 × 200 × 10 × 16 and H300 × 150 × 6.5 × 9, respectively. All of the column bases in the prototype buildings are designed as an embedded column base with a stiffness that meets the requirements of a rigid joint in the Eurocode (CEN 2005). Therefore, the column bases are fixed in the macromodel of the prototype buildings. Moreover, the fixed column bases are widely adopted in simulating the progressive collapse of steel frame buildings. For instance, the National Institute of Standards and Technology (NIST) designed two typical 10-story steel frame buildings to investigate effective designs in resisting disproportionate collapse, and the column bases were assumed as fixed (Sadek et al. 2010; Main and Sadek 2012). The composite slab and the floor beams are connected by 19-mm diameter shear studs. Each girder has 85 shear studs with a spacing of 100 mm, whereas each beam has 38 shear studs. A full shear connection is achieved between the composite slabs and the floor beams. Consequently, in the macromodel of the prototype buildings, the shear failure of the shear stud is not modeled. The section size of the steel braces in Building B is H175 × 175 × 7.5 × 11. In these prototype buildings, the steel properties used for the columns, beams, and girders are the same as those used in the girder flanges of the aforementioned composite floor specimen, whereas the material properties of the concrete, rebars, shear studs, and steel decks are identical to the composite floor specimen.

Using the calibration method for the connection springs previously mentioned, the axial spring parameters for the girder-to-column and beam-to-column connections are calibrated and listed in Table 2. The axial parameters of the web springs at the beam-to-girder connection are the same as that of the beam-to-column connection. Even though the shear failure mode of the moment-resisting connections has not been observed in the progressive collapse tests (Li et al. 2013, 2015; Qin et al. 2015; Wang et al. 2016, 2019a, b), the vertical shear failure is still simulated in prototype buildings. The vertical shear load is assumed to be merely resisted by the bolted shear tab connection, and the contribution of the flanges is neglected. The ultimate vertical shear resistance of each web spring is calculated by dividing the vertical ultimate capacity of the connection by the number of bolts. The vertical ultimate capacity of the connection is calculated according to the GB 50017-2017 (MOHURD 2017) specification. The vertical deformations of the web springs are neglected by defining a large vertical stiffness to them. When the ultimate vertical shear resistance or the axial fracture displacement is reached, the web springs are deleted from the model. For the girder-to-column and beam-to-column connections, the ultimate vertical shear resistance of the web springs is 235 kN and 91 kN, respectively. Because the top flanges of the girder and beam have been tightly restrained by the floor slab, the out-of-plane failure of the connection is not simulated in the model of the prototype buildings.

Analysis of Prototype Buildings

As indicated in Fig. 5, due to the symmetrical nature of the prototype building, there are nine single-column failure scenarios at the ground floor, namely, A1, A2, A3, B1, B2, B3, C1, C2, and C3. Using the macromodel previously verified, nonlinear static push-down analyses under these scenarios are performed. In the push-down analysis, the failed ground column is removed before the uniform vertical load is applied. Incrementally increasing the vertical load is uniformly applied on the floor slabs affected by the failed column and the floor slabs above it until the ultimate load-carrying capacity of the residual structure is reached. The total vertical reaction at the bases of all columns is considered as the building resistance. Dividing the building resistance by the floor area subjected to the vertical load is regarded as the load intensity. Therefore, the relationship between the load intensity and the vertical displacement at the failed column can be obtained.

Influence of Column Failure Location

Fig. 6 illustrates the load intensity-displacement relationship of Building A under different column removal scenarios. Table 3 summarizes the ultimate resistance of the Building A (R_A) under different column removal scenarios and compares them with the load combination for extraordinary events (1.2 DL + 0.5 LL), as defined in ASCE/SEI 7-16 (ASCE 2017) and that is called R_d in this study. As indicated in Table 3, R_A is much higher than its corresponding R_d for all column failure cases. The R_A of the C1 case is the highest, which is 4.90 R_d, whereas the B2 case has the lowest R_A, which is 3.27 R_d. For the A1, B1, and C1 cases, the R_A is at least equal to 4.27 R_d; for the other six cases excluding the C3 case, the R_A is approximately equal to 3.3 R_d. Compared with the other six cases, the tributary floor area of the affected girders of the A1, B1, and C1 cases is only half that of the other six cases, which causes the relatively higher R_A of these cases. Excluding the A1, B1, and C1 cases, the C3 case has slightly higher R_A than the other cases, which benefits from the development of the tensile membrane and two-way catenary actions after the surrounding horizontal boundaries

Table 2. Calibrated connection spring parameters for the macro models of prototype buildings

Connection type	Connection location	Spring	δ_y (mm)	t_y (kN)	δ_u (mm)	t_u (kN)	δ_0 (mm)
WFBW connection	Girder-to-column	Web spring	1.5	280	20	340	39
		Flange spring	0.02	1,354	2.05	1,818	2.55
	Beam-to-column	Web spring	1	125	13.5	160	16
		Flange spring	0.02	571	2	760	2.5
WFWW connection	Girder-to-column	Web spring	0.12	460	8	560	12
		Flange spring	0.06	1,354	0.6	1,747	0.8
	Beam-to-column	Web spring	0.1	200	12	260	14
		Flange spring	0.02	571	1	737	1.5

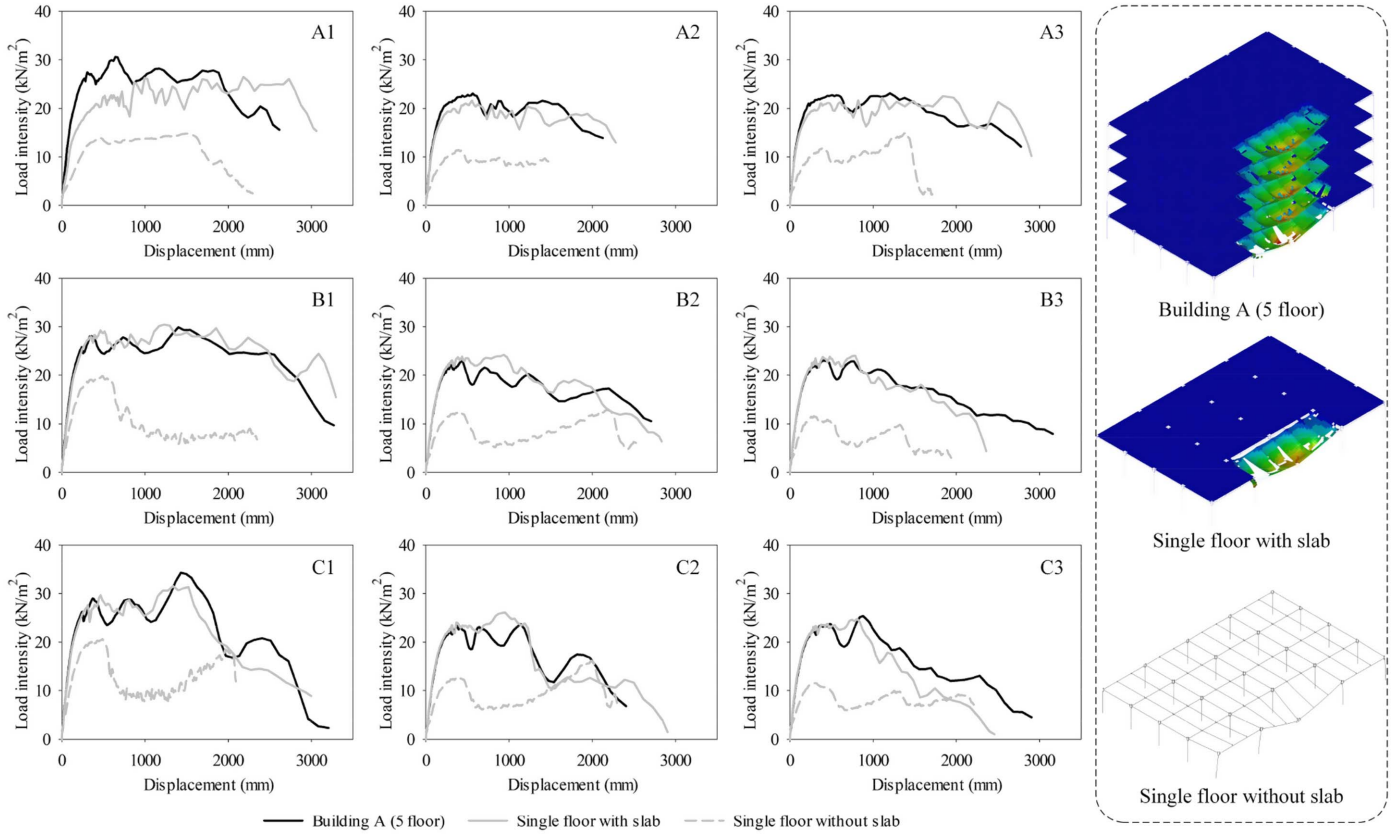

Fig. 6. Influences of column failure location, total number of floors, and floor slab.

Table 3. Ultimate resistance of prototype buildings

Removed column	1.2DL + 0.5LL	Building A		Single floor with slab		Single floor without slab		WFWW connection		Building B	
	R_d (kN/m^2)	R_A (kN/m^2)	R_A/R_d	R_{A1} (kN/m^2)	R_A/R_{A1}	R_{A1f} (kN/m^2)	R_{A1}/R_{A1f}	R_{AW} (kN/m^2)	R_A/R_{AW}	R_B (kN/m^2)	R_B/R_A
A1	7	30.61	4.37	26.51	1.15	14.82	1.79	29.64	1.03	40.07	1.31
A2	7	23.07	3.30	21.62	1.07	11.43	1.89	22.84	1.01	38.42	1.67
A3	7	23.12	3.30	22.51	1.03	14.92	1.51	23.24	0.99	36.05	1.56
B1	7	29.88	4.27	30.45	0.98	19.86	1.53	30.33	0.99	38.64	1.29
B2	7	22.87	3.27	24.22	0.94	12.98	1.87	22.11	1.03	22.92	1.00
B3	7	23.11	3.30	24.04	0.96	11.54	2.08	22.82	1.01	23.51	1.02
C1	7	34.29	4.90	31.54	1.09	20.61	1.53	31.46	1.09	33.62	0.98
C2	7	23.70	3.39	26.13	0.91	16.18	1.62	22.54	1.05	40.37	1.70
C3	7	25.36	3.62	24.77	1.02	11.57	2.14	23.52	1.08	42.11	1.66

are constrained. For the B2 and B3 cases, limited by the weak horizontal constraints, the tensile membrane and catenary actions cannot be fully developed at the large deformation stage; therefore, the load intensity-displacement curves of these two cases indicate an obvious downward trend after reaching their maximum flexural resistance. According to Li et al. (2013, 2015), the catenary force in the steel beam begins to develop when the beam's chord rotation exceeds 0.1 rad. Therefore, this deformation (0.1 rad, 900 mm) is taken as the starting point of the large deformation stage in this study.

Influence of Total Number of Floors

To study the influence of the total number of floors on the progressive collapse resistance, the ground floor in Building A is extracted to investigate its structural responses under different column removal scenarios, and the corresponding load intensity-displacement curves are drawn in Fig. 6. Except for the A1 case, the load intensity-displacement curves of the five- and single-story prototype structures are approximately the same. Table 3 summarizes the ultimate resistance of the single-floor prototype structure (R_{A1}) for each column removal scenario and compares it with the corresponding R_A. Except for the A1 case, the differences between R_A and R_{A1} for the rest of the cases are less than 10%. For the A1 case, the R_A is 1.15 times R_{A1} because the five-story structure develops the Vierendeel mechanism, which is lacking in the single-story structure (Sagiroglu and Sasani 2014; Qiao et al. 2018). Apart from the corner column loss scenario (A1), the influence of the Vierendeel mechanism on the load-carrying capacity of building A is

negligible. This finding indicates that the load carried by each floor in building A is almost the same; in other words, the vertical load of the multistory structure under the column loss scenario is not concentrated on a certain floor. Therefore, if the structural arrangement, size, and applied gravity load of each floor are the same, each floor tends to resist only the vertical load applied to it. This conclusion echoes the finding reported by Hoffman and Fahnestock (2011). Hence, except for the corner column failure scenario, the total number of floors does not significantly change the performance of the regular structure under progressive collapse scenario.

Influence of Composite Floor Slab

To study the effect of the composite floor slab on the progressive collapse resistance, the floor slab in the single-floor structure is removed to make it become a single-floor frame, and the vertical displacement-controlled load is applied to the failed column. The load intensity of the single-floor frame is calculated by dividing the total vertical resistance by the tributary floor area of the removed column. For instance, the tributary floor area of the A1 case equals 13.5 m^2 (0.5 girder span × 0.5 beam span), which is only a quarter of the loading area for the single-floor structure with a slab. Fig. 6 depicts the load intensity-displacement curves of different column failure cases. Table 3 summarizes the ultimate resistance of the single-story structure without a slab (R_{A1f}) under each column removal scenario and compares it with the corresponding R_{A1}. The conclusion reached is that the composite floor slab can increase the R_{A1f} by at least 51% and even increase it by 114% for the C3 case. Furthermore, the minimum R_{A1} (21.62 kN/m^2) is 89% higher than the minimum R_{A1f} (11.43 kN/m^2). This finding implies that the composite floor slab can greatly improve the progressive collapse resistance of the steel frame structure; therefore, the contribution of the composite floor slab cannot be ignored in the progressive collapse resistance analysis of the steel frame structure.

Influence of Beam-to-Column Connection Type

In this section, the effects of two commonly used rigid beam-to-column connections, including WFBW and welded flange-welded web (WFWW) connections, on the progressive collapse resistance of Building A are studied. The Complete-Joint-Penetration groove weld is used to connect the flanges, webs, and shear tabs to the column wall. The strength of the weld is assumed to be stronger than the connected members, and the influence of the weld on the surrounding materials is neglected.

First, the bearing and deformation capacities of these two connections are compared using the solid element half-span model [Fig. 2(d)], and the corresponding simulation results of the beam-to-column and girder-to-column connections are indicated in Fig. 7(a). For the beam-to-column connection, the vertical displacement corresponding to the ultimate resistance of the WFBW connection is 144% higher than that of the WFWW connection, but its ultimate resistance is 8.2% lower than that of the WFWW connection. For the girder-to-column connection, the vertical displacement corresponding to the ultimate resistance of the WFBW connection is 147% higher than that of the WFWW connection, but the ultimate resistance is reduced by 6.8% compared with the WFWW connection. Despite the fact that the ultimate resistance of the WFWW connection is slightly higher, the WFBW connection has an obvious advantage in developing catenary action at the large deformation stage, which is also confirmed by the experimental test conducted by Li et al. (2013). For the macromodel of the WFWW connection, the modeling method of the flanges is the same as that of the WFBW connection, whereas the welded webs are divided equally into four pieces and simulated by four web springs, as indicated in Fig. 7(b). Using a similar calibration approach as that used for the WFBW connection, the connection springs of the WFWW connection are calibrated, and the axial parameters of springs are listed in Table 2. In addition, for the girder-to-column WFWW and beam-to-column WFWW connections, the ultimate vertical shear resistance of the web spring is 310 kN and 131 kN, respectively.

After replacing the WFBW connection in building A with the WFWW connection, the load intensity-displacement curves corresponding to each column failure case are drawn in Fig. 7(c). Table 3 summarizes the ultimate resistance of Building A using the WFWW connection (R_{AW}) in each column failure case and compares it with the ultimate resistance of Building A using the WFBW connection (R_A). Except for the C1, C2, and C3 cases, R_{AW} and R_A are approximately equal. For the C1, C2, and C3 cases, R_A is 9%, 5%, and 8% higher than the corresponding R_{AW}. For these three cases, the horizontal boundary displacement of girders is constrained by the adjacent structures, which contributes to the development of the catenary action in the building using the WFBW connection. In addition, as indicated in Fig. 7(c), except for the A1 and B1 cases, the load-carrying capacity of Building A with the WFBW connection is significantly higher than that using the WFWW connection at the large deformation stage. Therefore, for the steel frame buildings, the progressive collapse resistance of the WFBW connection is superior to that of the WFWW connection.

Influence of Steel Braces

Fig. 8(a) provides the macromodel of Building B and the modeling approach for the steel braces. Steel braces are modeled using the Hughes-Liu beam elements, and the connection regions are represented by rigid bars. The braces are fully constrained to the rigid bars to simulate the rigid connections between them.

Given the observation of the failure phenomenon, the failure modes of Building B can be classified into two categories: (1) floor failure caused by the connection failure and slab fracture, and (2) column failure caused by the redistributed vertical load and P-delta effect. The failure modes of C1 and C3 cases of Building B are floor failure and column failure, respectively. The load intensity-displacement curves of Building A and Building B are drawn in Fig. 8(b). Table 3 summarizes the primary simulation results of Building A and Building B. Except for the B2, B3, and C1 cases, the ultimate resistance of Building B (R_B) is significantly higher than the corresponding R_A. C2 case has the largest improved percentage (70%), and B1 case has the least (29%). For the B2, B3, and C1 cases, the load intensity-displacement curves of Building A and Building B are nearly the same because Building B has no braces located in the affected spans for these cases. In contrast, for the remaining cases, the steel braces located in the affected spans have significantly enhanced the ultimate vertical resistance (at least by 29%) and reduced the vertical deformation. Compared with Building A, the steel braces in Building B changed the failure modes of the C2 and C3 cases from floor failure to column failure. The column failure mode indicates that the structure reached the maximum vertical resistance that can be achieved under this case, whereas the floor failure mode indicates that the vertical load of the structure is inadequate to cause the column failure.

Influence of Adjacent Spans

At the girder/beam-to-column connection and composite slab levels, the stiffness of the horizontal boundary constraints can significantly change the progressive collapse behavior (Kang et al. 2017; Wang et al. 2021). When an entire structure is subjected to column

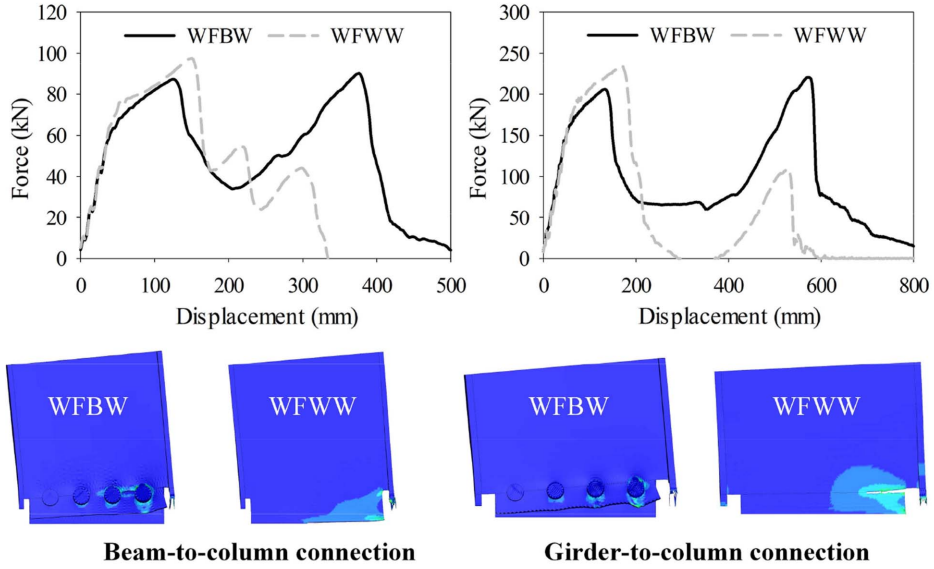

(a)

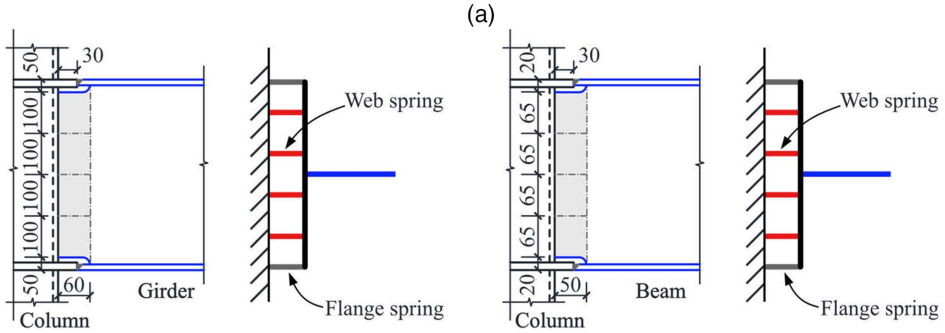

(b)

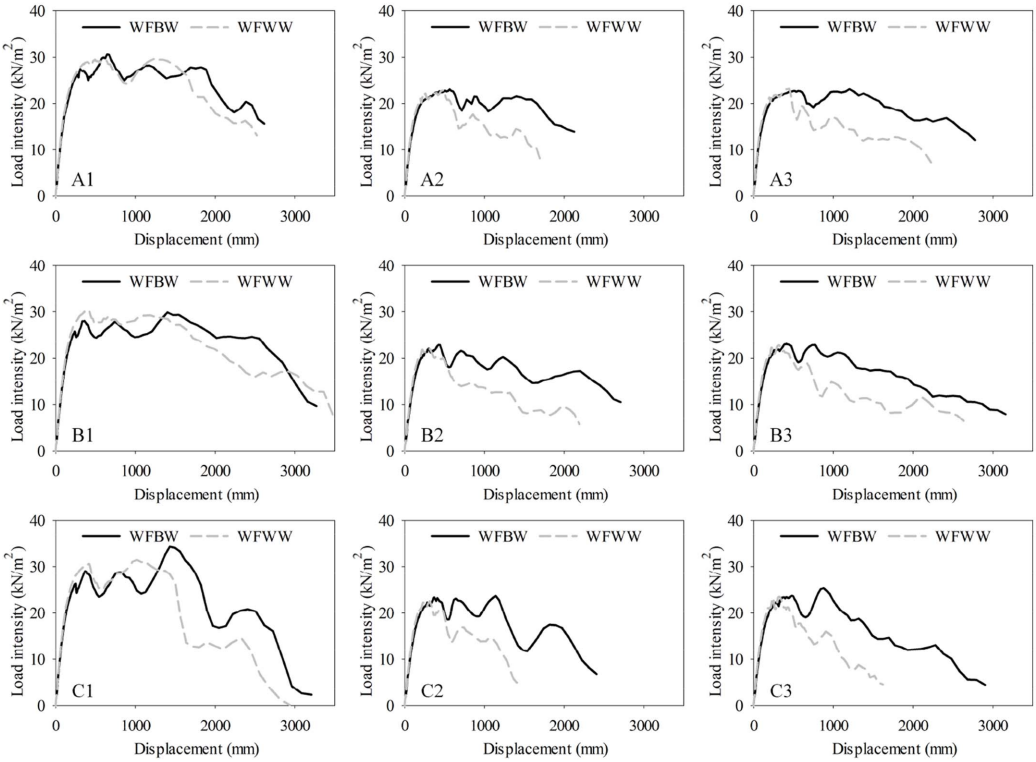

(c)

Fig. 7. Influences of connection type.

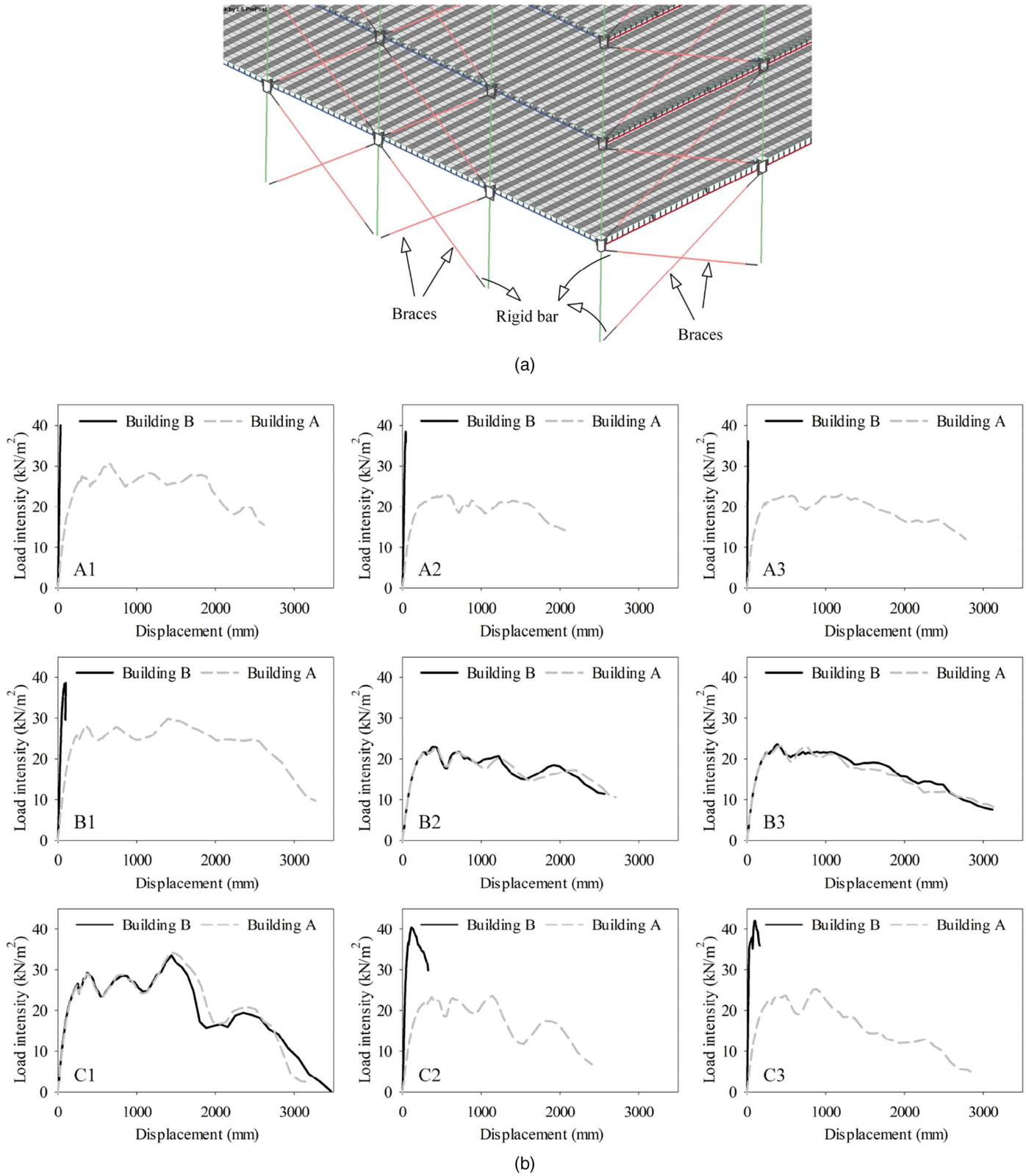

Fig. 8. Influences of steel braces.

loss, the horizontal boundary constraints of the affected floor region are provided by its adjacent spans. As indicated in Fig. 9, based on the C1 and C3 cases in Building A, the effect of adjacent spans on the progressive collapse response is studied. A total of four cases are compared and analyzed: without adjacent span, one adjacent span, two adjacent spans, and three adjacent spans. The deformation modes and load intensity-displacement curves corresponding to these circumstances are indicated in Fig. 9.

Fig. 9 indicates that the adjacent spans can alter the progressive collapse resistance at the large deformation stage, whereas the

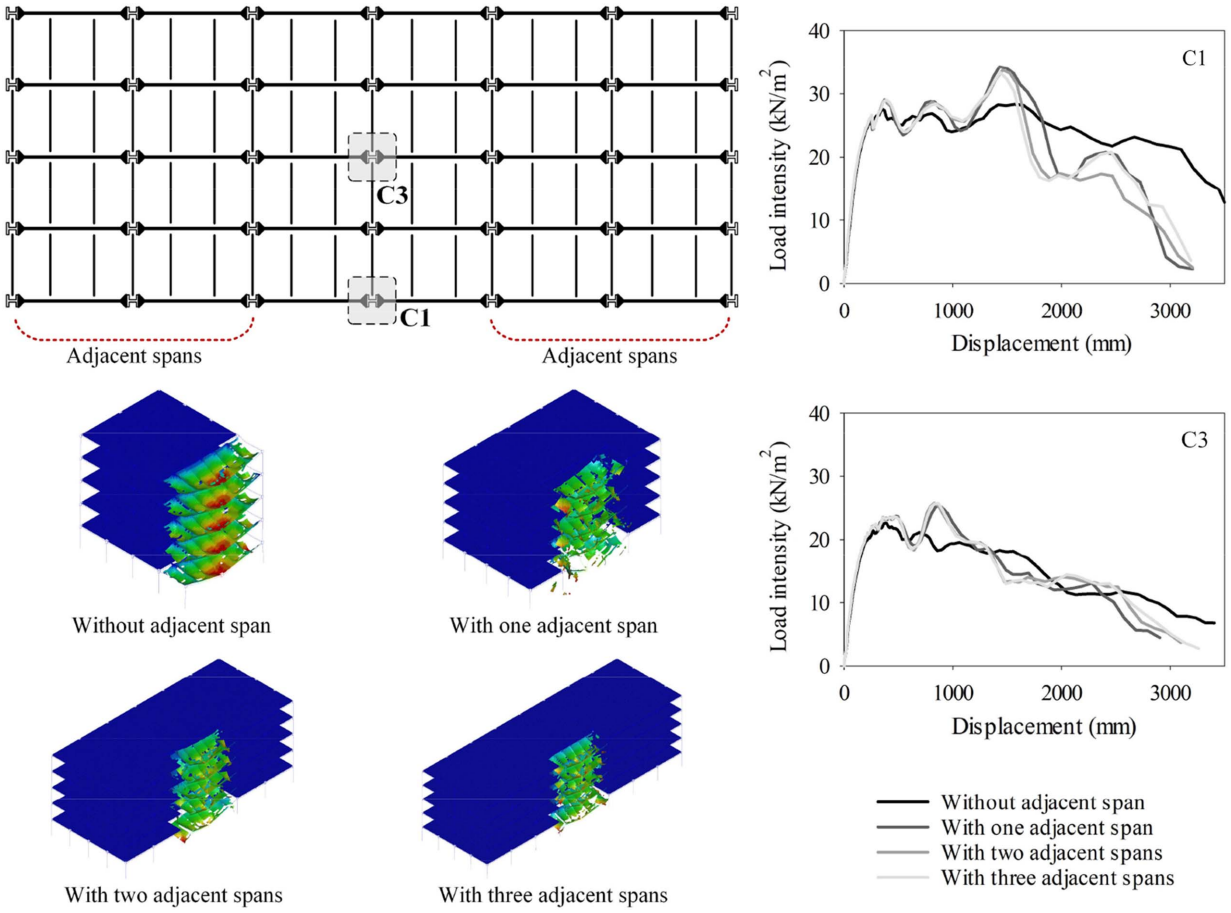

Fig. 9. Influence of adjacent spans.

structural response at the flexural stage is not affected. For the C1 case, the ultimate resistance of one adjacent span circumstance is 21% higher than that of the circumstance without an adjacent span because obvious catenary and tensile membrane actions are developed with the help of an adjacent span. For the circumstance without an adjacent span, compared with its flexural capacity, no obvious increase occurs in the load-carrying capacity at the large deformation stage. However, for circumstances with one, two, or three adjacent spans, the load intensity-displacement curves are approximately the same. With respect to the C3 case, a similar phenomenon is observed, and the ultimate resistance of cases with adjacent spans is approximately 12% higher than that of the case without adjacent spans. The conclusion reached is that adjacent spans can improve the progressive collapse resistance by improving the catenary and tensile membrane actions. For Building A, one adjacent span is sufficient for developing the catenary and tensile membrane actions.

Robustness Evaluation and Enhancement Strategies

Robustness Evaluation Method

Through the aforementioned macromodeling approach, the nonlinear static response of the steel frame buildings under column loss scenarios can be obtained. As indicated in Fig. 10(a), based on the energy-based method proposed by Izzuddin et al. (2008), the nonlinear static response can be converted into an equivalent dynamic response. After reaching the static ultimate capacity (F_{su}), the load-carrying capacity of the structure becomes unstable and might suddenly break down (Main 2014; Bao et al. 2017). Therefore, the displacement corresponding to F_{su} is regarded as the termination point of the equivalent dynamic response curve. Before this termination point, the dynamic ultimate capacity (F_{du}) achieved by the equivalent dynamic response curve can be regarded as the structure's ultimate capacity against progressive collapse.

Fig. 10(b) depicts the structural robustness evaluation method and design routine of the steel frame building. The minimum F_{du} of all column loss scenarios is regarded as the ultimate capacity of the objective structure. The progressive collapse resistance demand of this structure is chosen as the load combination for extraordinary events R_d, which is specified in ASCE/SEI 7-16 (ASCE 2017). If the ultimate capacity of the objective structure is higher than its progressive collapse resistance demand, this structure is considered to be robust enough to avoid a progressive collapse. Otherwise, selecting an appropriate structural robustness enhancement method to redesign and re-evaluate the objective structure is necessary until its ultimate capacity is higher than its progressive collapse resistance demand.

Retrofitted Moment Resisting Connection

Fig. 11(a) illustrates a retrofitted moment-resisting connection with steel strands, which can enhance structural robustness by providing a second line of defense to the girder-to-column and beam-to-column connections. This proposed connection comprises columns, girders, beams, steel strands, and stiffening ribs. The yield strength, ultimate strength, and ultimate strain of the steel strand are 1,800 MPa, 1,900 MPa, and 0.05, respectively. The girder-to-column connection in Wang et al. (2019b) is chosen here to establish this

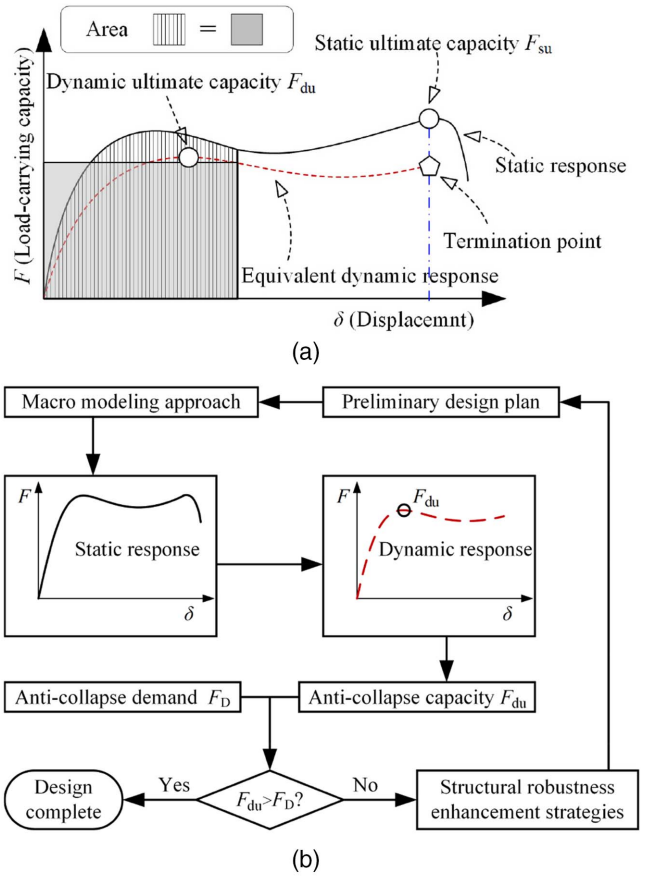

Fig. 10. Structural robustness evaluation method.

retrofitted connection. Four steel strands are installed in this connection region for which the yield capacity equals the girder section. The cross-section area of each strand is 98.7 mm^2. Fig. 11(a) indicates the half-span model with the retrofitted moment-resisting connection, a modeling strategy that follows that used by Wang et al. (2019b). Steel strands are modeled by truss elements, the ends of which are coupling with the corresponding girder section to simulate the constraints from stiffening ribs.

Using this model, as indicated in Fig. 11(a), the influences of the length and prestress of the steel strand are investigated. After installing steel strands, the vertical resistance of the half-span model is remarkably improved. When the strand length in the half-span model (l_s) equals three times the girder height (h_f), the vertical resistance is highest, which is 3.66 times the model without a steel strand. Moreover, the deformation capacity of this connection is also improved by 198%. Therefore, the strand length $l_s = 3h_f$ is selected in the following simulations. As indicated in Fig. 11(a), the ratio between strand prestress and its yield stress (β) has a limited impact on the vertical resistance of the half-span model. Therefore, in the following simulation, the steel strands are not applied prestress.

The girder-to-column and beam-to-column connections in Building A are all replaced by the retrofitted moment-resisting connection. This reinforced building is called Building C. In Building C, four steel strands (cross-section area of each strand is 406.5 mm^2) are installed in the girder-to-column connection, and four steel strands (cross-section area of each strand is 165.0 mm^2) are installed in the beam-to-column connection. As indicated in Fig. 11(b), the steel strands in the macromodel are modeled by truss elements, and the cross-section area of each truss element equals the sum of the cross-section area of the two steel strands at the same elevation. The size of the truss element is 50 mm. In the macromodel, one end of the steel strand is constrained to the beam through a rigid bar, and the other end is fixed to the connection region at its corresponding elevation.

Fig. 11(c) indicates the load intensity-displacement curves of Building C subjected to different column loss scenarios. Its ultimate resistance (R_C) is listed in Table 4. Given o the retrofitted connection, R_C exceeds its corresponding R_A under all column removal cases. For Building A, the progressive collapse resistance of the A2, A3, B2, B3, C2, and C3 cases are comparatively weak. After replacing with the retrofitted connection, the ultimate resistance of these six cases has been improved by at least 11%, and this A3 case percentage reaches 24%. The improvement in the progressive collapse resistance of these cases is attributed to the enhanced catenary action. Compared with Building A, the improvement percentage of the A1 case is the lowest in Building C, at only 3%. This is because the progressive collapse resistance under the corner column removal scenario is mainly provided by the flexural capacity of the beams and slabs and the Vierendeel mechanism between the different floors. Therefore, for the A1 case, the advantage of the retrofitted connection in developing catenary action cannot be exerted.

According to the method depicted in Fig. 10(a), the nonlinear static response curves of Building A and Building C in Fig. 11(c) are converted into equivalent dynamic response curves. The dynamic ultimate capacity of Buildings A and C is summarized in Table 4 and is denoted by F_{du_A} and F_{du_C}, respectively. For Building A, the R_A of the A2, A3, B2, B3, C2, and C3 cases is relatively weak. However, after being converted into a dynamic response, F_{du_A} of the B2 and B3 cases is much weaker than that of the A2, A3, C2, and C3 cases because when the static response reaches its ultimate resistance, the displacements of the B2 and B3 cases are relatively small, and their equivalent dynamic response curves are more similar to the "Type 1" dynamic response curve, which is discussed in the next section. The F_{du_A} of the B2 and B3 cases, which are the most vulnerable cases in Building A, is approximately 2.45 times the corresponding R_d. Therefore, Building A is concluded as having sufficient structural robustness to prevent the progressive collapse initiated by a single ground floor column failure. By comparing F_{du_A} and F_{du_C}, the dynamic ultimate capacity has been improved for all cases when the retrofitted connections are utilized. For Building C, the most vulnerable cases are still the interior column removal cases, including the B2, B3, C2, and C3 cases, but the F_{du_C} of these cases is at least 2.92 times the corresponding R_d. Therefore, compared with the minimum F_{du_A} in Building A, the minimum dynamic ultimate capacity of Building C has been improved by 19%.

Discussion of Robustness Enhancement Strategies

Using the energy-based method depicted in Fig. 11(c), the dynamic ultimate capacity of the aforementioned nonlinear static pushdown analyses is obtained, which is indicated in Fig. 12(a). For the "single floor without slab," the dynamic ultimate capacity of the A2, B3, and C3 cases is closest to R_d [the dashed line in Fig. 12(a)], which is on the very edge of progressive collapse. Consequently, preventing progressive collapse merely relying on the steel frame without improvements is difficult. The minimum dynamic ultimate capacity of "single floor with slab" (21.62 kN/m^2) is 2.14 times that of "single floor without slab" (7.96 kN/m^2). This finding indicates that, with the help of the composite slab, the structural robustness of the steel frame has more than doubled. The minimum dynamic ultimate capacity of Building A (17.12 kN/m^2) is 7%

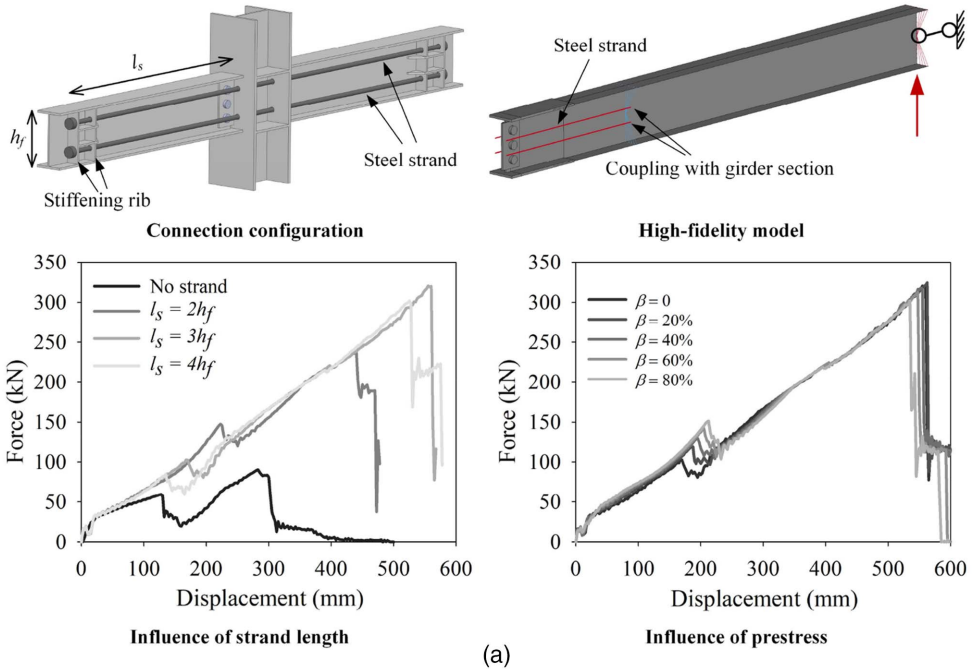

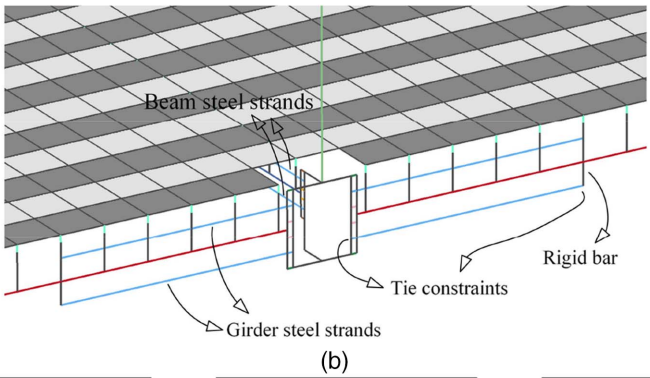

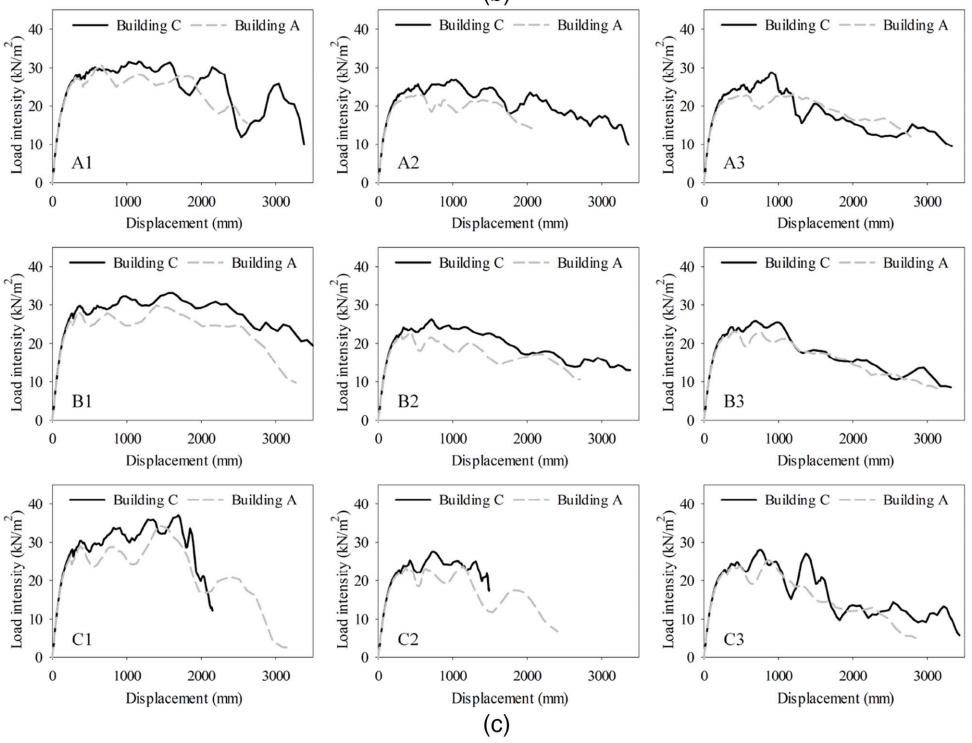

Fig. 11. Retrofitted moment-resisting connection.

Table 4. Static and dynamic ultimate resistance of Building C and Building A

Removed column	1.2DL + 0.5LL	Building A			Building C			
	R_d (kN/m^2)	R_A (kN/m^2)	F_{du_A} (kN/m^2)	F_{du_A}/R_d	R_C (kN/m^2)	F_{du_C} (kN/m^2)	R_C/R_A	F_{du_C}/F_{du_A}
A1	7	30.61	23.22	3.32	31.67	26.66	1.03	1.15
A2	7	23.07	18.67	2.67	26.81	22.14	1.16	1.19
A3	7	23.12	20.22	2.89	28.76	22.27	1.24	1.10
B1	7	29.88	24.58	3.51	33.08	28.07	1.11	1.14
B2	7	22.87	17.12	2.45	26.27	20.45	1.15	1.19
B3	7	23.11	17.27	2.47	25.80	20.49	1.12	1.19
C1	7	34.29	25.41	3.63	37.00	29.86	1.08	1.18
C2	7	23.70	19.84	2.83	27.58	20.79	1.16	1.05
C3	7	25.36	19.98	2.85	28.04	21.17	1.11	1.06

higher than that of the building with the WFWW connection (16.02 kN/m^2); thus, the WFBW connection is better than the WFWW connection in preventing progressive collapse.

As is noted in the preceding section, after replacing all of the girder-to-column connections and beam-to-column connections in Building A by the retrofitted connections, the structural robustness improved by 19%. As indicated in Fig. 12(a), except for the C2 and C3 cases, the dynamic ultimate capacity of all of the cases was noticeably improved. The ineffectiveness of the retrofitted connection for the C2 and C3 cases is mainly attributable to the slab fracture. For Building A, the failure of the C2 and C3 cases is the result of the slab fracture, which cuts off the load paths between slabs and girders and between slabs and beams. Therefore, the advantage of the retrofitted connection cannot be developed if the slab load cannot transfer to the girders and beams. Although the resistance of the B2 and B3 cases was improved by the retrofitted connection, the dynamic ultimate capacity of these two cases has yet to exceed that of the C2 and C3 cases, which is also limited by the slab fracture. Given this, for the interior column removal scenarios, improving the tensile membrane action of a slab rather than merely improving the catenary action of the girders and beams would be more practical. As noted by Wang et al. (2021), improving the continuity of the steel deck can be selected as an appropriate choice.

Moreover, as indicated in Fig. 12(a), the steel braces significantly improved the dynamic ultimate capacity of the C2 and C3 cases. However, for the A1 and A3 cases, the dynamic ultimate capacity was even weakened by the steel braces. This phenomenon can be explained by Fig. 12(b). As depicted by the "Type 1" in Fig. 12(b), if the static response curve is a straight line, the equivalent dynamic response is also a straight line, and F_{du} will equal $0.5F_{su}$. However, if the static response curve is convex downward, as depicted by the "Type 2" in Fig. 12(b), its corresponding F_{du} will be larger than $0.5F_{su}$. Therefore, if the F_{su} is the same for "Type 1" and "Type 2", the F_{du} of "Type 2" will be higher than that of "Type 1." As indicated in Fig. 8(b), the static load intensity-displacement curves of the A1, A2, and A3 cases are more similar to those of "Type 1," and the F_{su}/F_{du} ratios of these cases approximately equal 2 (Fig. 12b). Hence, although the static ultimate capacity of these cases improved by more than 31% (Table 3), the dynamic ultimate capacity might be weakened. For the C2 and C3 cases in Building B, the static load intensity-displacement curves are still "Type 2," and the F_{su}/F_{du} ratios range from 1.27 to 1.40. In this situation, the steel braces improve the dynamic ultimate capacity by at least 45%. The results in Fig. 12 lead to the conclusion that the steel braces cannot be placed at the exterior frames or connected to the exterior columns. Because the redistributed vertical load to the removed exterior columns is comparatively less, the removed exterior columns supported by the steel braces might not be able to develop much vertical displacement, which would change the static response curves from "Type 2" to "Type 1." Therefore, placing the steel braces at spans not connected with the exterior columns is better.

Conclusions

This study presents a macromodeling approach that is applicable to analyze the progressive collapse behavior of steel frame buildings with the composite slab. This modeling approach can accurately account for the local steel fracture and concrete damage behavior without losing computational efficiency. This modeling approach is verified by comparing its results with a full-scale composite floor test; then, it is applied to the progressive collapse simulation of a specially designed fivee-story prototype building. Based on this building, the influence of some key factors, including column failure location, total number of floors, floor slab, beam-to-column connection type, adjacent span, and steel brace, on collapse resistance are investigated. Thereafter, the structural robustness of the prototype building is assessed. Meanwhile, a retrofitted moment-resisting connection with steel strands is proposed and applied to the prototype building. The effectiveness of this developed connection in enhancing structural robustness is validated. Finally, based on the obtained analysis results, the following conclusions are reached.

- In steel frame buildings with a composite slab, the progressive collapse resistance is lower when the inner and beam side columns are removed, whereas the progressive collapse resistance is comparatively higher when corner or girder side columns fail.
- Except for the corner column loss scenario, the total number of floors of Building A has a negligible effect on the progressive collapse resistance, echoing the finding reported by Hoffman and Fahnestock (2011). Noteworthy is that for the prototype building investigated in this study, the floor slab geometry, floor beam configuration, column dimension, designed floor load, and floor height do not changed over the building height. Any change in these conditions might potentially affect the accuracy of this conclusion. Under the corner column loss scenario, the Vierendeel mechanism developed between different floors is a benefit for the progressive collapse resistance.
- The composite floor slab can increase the minimum dynamic ultimate capacity of Building A investigated in this study by 114%. Therefore, the contribution of composite floor slabs needs to be carefully considered in the analysis of the progressive collapse behavior of steel frame buildings.
- Compared with the WFWW connection, the WFBW connection investigated in this study can improve the minimum dynamic ultimate capacity of the prototype building by 7%. Moreover, the load-carrying capacity of Building A at the large deformation stage was also improved.
- Adjacent spans can improve the progressive collapse resistance by improving the catenary and tensile membrane actions.

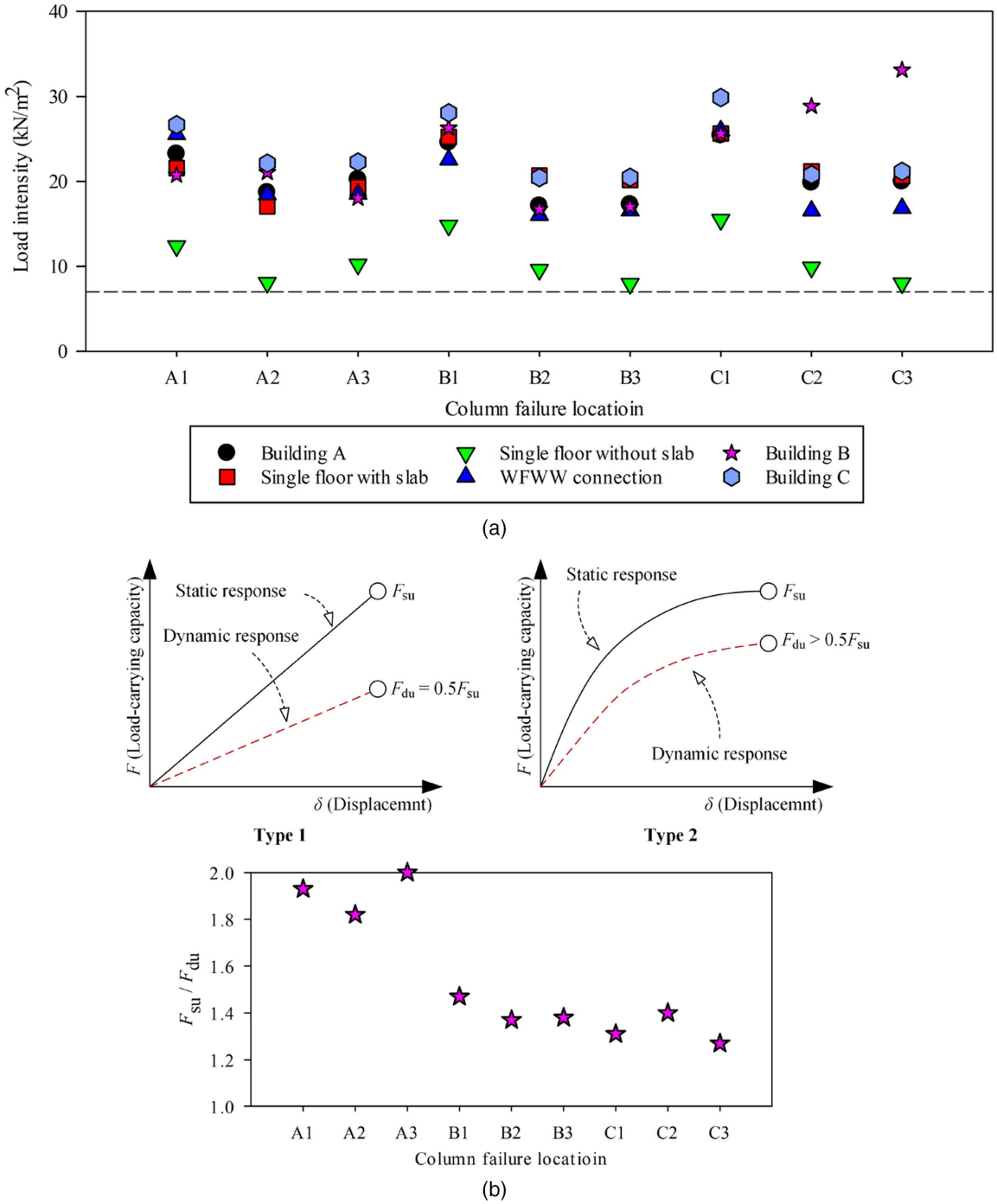

Fig. 12. Structural robustness comparisons.

For Building A, one adjacent span is sufficient for developing the catenary and tensile membrane actions.

- The minimum dynamic ultimate capacity of Building A is approximately 2.45 times the corresponding R_d. Building A has sufficient structural robustness to prevent the progressive collapse initiated by a single ground floor column failure.
- If the removed column is located in the affected spans, the steel braces can improve the static ultimate capacity by at least 29%. However, steel braces might be harmful to the sudden exterior column removal scenarios. Placing the steel braces at the spans not connected with the exterior columns is preferred.
- The proposed retrofitted moment-resisting connection can improve the progressive collapse resistance of the girder-to-column connection by 266%. The progressive collapse resistance of the retrofitted connection is highest when $l_s = 3h_f$, where l_s is the distance from the column flange to the anchored end of the strand, and h_f is the girder height. The prestress in the steel strand has no obvious influence on the load-carrying and deformation capacities of the retrofitted connection. After installing the retrofitted connection, the dynamic ultimate resistance of the prototype building is improved by 19%.

Interesting to note is that, although the ultimate capacity of the girder-to-column connection is increased by 266% by using the

retrofitted connection, it can only improve the overall capacity of the prototype building by 19%. However, given the contribution of the composite slab, the overall capacity of the prototype building is increased by 114%. Therefore, focusing on improving the contribution of the floor slab would be more sensible than merely enhancing the connection performance.

Data Availability Statement

Some or all of the data, models, or code that support the findings of this study are available from the corresponding author on reasonable request.

Acknowledgments

The research work in this paper was sponsored by the State Key Laboratory of Diaster Reduction in Civil Engineering (Tongji University, No. SLDRCE19-A-03) and the Natural Science Foundation of China (No. 51378380).

References

Alashker, Y., S. El-Tawil, and F. Sadek. 2010. "Progressive collapse resistance of steel-concrete composite floors." *J. Struct. Eng.* 136 (10): 1187–1196. https://doi.org/10.1061/(ASCE)ST.1943-541X.0000230.

Alashker, Y., H. Li, and S. El-Tawil. 2011. "Approximations in progressive collapse modeling." *J. Struct. Eng.* 137 (9): 914–924. https://doi.org/10.1061/(ASCE)ST.1943-541X.0000452.

ASCE. 2017. *Minimum design loads and associated criteria for buildings and other structures*. ASCE/SEI 7-16. Reston, VA: ASCE.

Bao, Y., J. A. Main, and S. Y. Noh. 2017. "Evaluation of structural robustness against column loss: Methodology and application to RC frame buildings." *J. Struct. Eng.* 143 (8): 04017066. https://doi.org/10.1061/(ASCE)ST.1943-541X.0001795.

CEN (European Committee for Standardization). 2005. *Eurocode 3: Design of steel structures, Part 1-8: Design of joints*. EN 1993-1-8. Brussels, Belgium: CEN.

CEN (European Committee for Standardization). 2006. *Eurocode 1: Actions on structures, part 1-7: General actions—Accidental actions*. EN 1991-1-7. Brussels, Belgium: CEN.

CPNI (Centre for the Protection of National Infrastructure). 2011. *Review of international research on structural robustness and disproportionate collapse*. London: Department for Communities and Local Government.

Ding, Y., X. Song, and H. T. Zhu. 2017. "Probabilistic progressive collapse analysis of steel-concrete composite floor systems." *J. Constr. Steel Res.* 129 (Feb): 129–140. https://doi.org/10.1016/j.jcsr.2016.11.009.

DoD (Department of Defense). 2016. *Design of buildings to resist progressive collapse*. UFC 4-023-03. Washington, DC: DoD.

Fu, F. 2009. "Progressive collapse analysis of high-rise building with 3-D finite element modeling method." *J. Constr. Steel Res.* 65 (6): 1269–1278. https://doi.org/10.1016/j.jcsr.2009.02.001.

Fu, F. 2010. "3-D nonlinear dynamic progressive collapse analysis of multi-storey steel composite frame buildings—Parametric study." *Eng. Struct.* 32 (12): 3974–3980. https://doi.org/10.1016/j.engstruct.2010.09.008.

GSA (General Services Administration). 2016. *Alternate path analysis & design guidelines for progressive collapse resistance*. Washington, DC: GSA.

Hadjioannou, M., S. Donahue, E. B. Williamson, and M. D. Engelhardt. 2018. "Large-scale experimental tests of composite steel floor systems subjected to column loss scenarios." *J. Struct. Eng.* 144 (2): 04017184. https://doi.org/10.1061/(ASCE)ST.1943-541X.0001929.

Hoffman, S. T., and L. A. Fahnestock. 2011. "Behavior of multi-story steel buildings under dynamic column loss scenarios." *Steel Compos. Struct.* 11 (2): 149–168. https://doi.org/10.12989/scs.2011.11.2.149.

Izzuddin, B. A., A. G. Vlassis, A. Y. Elghazouli, and D. A. Nethercot. 2008. "Progressive collapse of multi-storey buildings due to sudden column loss—Part I: Simplified assessment framework." *Eng. Struct.* 30 (5): 1308–1318. https://doi.org/10.1016/j.engstruct.2007.07.011.

Johnson, E. S., J. E. Meissner, and L. A. Fahnestock. 2016. "Experimental behavior of a half-scale steel concrete composite floor system subjected to column removal scenarios." *J. Struct. Eng.* 142 (2): 04015133. https://doi.org/10.1061/(ASCE)ST.1943-541X.0001398.

Kang, S. B., K. H. Tan, H. Y. Liu, X. H. Zhou, and B. Yang. 2017. "Effect of boundary conditions on the behaviour of composite frames against progressive collapse." *J. Constr. Steel Res.* 138 (Nov): 150–167. https://doi.org/10.1016/j.jcsr.2017.07.005.

Khandelwal, K., and S. El-Tawil. 2011. "Pushdown resistance as a measure of robustness in progressive collapse analysis." *Eng. Struct.* 33 (9): 2653–2661. https://doi.org/10.1016/j.engstruct.2011.05.013.

Kwasniewski, L. 2010. "Nonlinear dynamic simulations of progressive collapse for a multi-story building." *Eng. Struct.* 32 (5): 1223–1235. https://doi.org/10.1016/j.engstruct.2009.12.048.

Li, H., and S. El-Tawil. 2014. "Three-dimensional effects and collapse resistance mechanisms in steel frame buildings." *J. Struct. Eng.* 140 (8): A4014017. https://doi.org/10.1061/(ASCE)ST.1943-541X.0000839.

Li, L., W. Wang, Y. Chen, and Y. Lu. 2013. "Experimental investigation of beam-to-tubular column moment connections under column removal scenario." *J. Constr. Steel Res.* 88 (Sep): 244–255. https://doi.org/10.1016/j.jcsr.2013.05.017.

Li, L., W. Wang, Y. Chen, and Y. Lu. 2015. "Effect of beam web bolt arrangement on catenary behaviour of moment connections." *J. Constr. Steel Res.* 104 (Jan): 22–36. https://doi.org/10.1016/j.jcsr.2014.09.016.

Main, J. A. 2014. "Composite floor systems under column loss: Collapse resistance and tie force requirements." *J. Struct. Eng.* 140 (8): A4014003. https://doi.org/10.1061/(ASCE)ST.1943-541X.0000952.

Main, J. A., and F. Sadek. 2012. *Robustness of steel gravity frame systems with single-plate shear connections*. Washington, DC: US Department of Commerce.

MOHURD (Ministry of Housing and Urban-Rural Development of the People's Republic of China). 2010. *Code for seismic design of buildings*. GB 50011-2010. Beijing: MOHURD.

MOHURD (Ministry of Housing and Urban-Rural Development of the People's Republic of China). 2017. *Standard for design of steel structures*. GB 50017-2017. Beijing: MOHURD.

Qiao, H., Y. Yang, and J. Zhang. 2018. "Progressive collapse analysis of multistory moment frames with varying mechanisms." *J. Perform. Constr. Facil.* 32 (4): 04018043. https://doi.org/10.1061/(ASCE)CF.1943-5509.0001192.

Qin, X., W. Wang, Y. Chen, and Y. Bao. 2015. "Experimental study of through diaphragm connection types under a column removal scenario." *J. Constr. Steel Res.* 112 (Sep): 293–304. https://doi.org/10.1016/j.jcsr.2015.05.022.

Sadek, F., S. El-Tawil, and H. Lew. 2008. "Robustness of composite floor systems with shear connections: modeling, simulation, and evaluation." *J. Struct. Eng.* 134 (11): 1717–1725. https://doi.org/10.1061/(ASCE)0733-9445(2008)134:11(1717).

Sadek, F., J. A. Main, H. S. Lew, S. D. Robert, V. P. Chiarito, and S. El-Tawil. 2010. *An experimental and computational study of steel moment connections under a column removal scenario*. Washington, DC: US Department of Commerce.

Sagiroglu, S., and M. Sasani. 2014. "Progressive collapse-resisting mechanisms of reinforced concrete structures and effects of initial damage locations" *J. Struct. Eng.* 140 (3): 04013073. https://doi.org/10.1061/(ASCE)ST.1943-541X.0000854.

Starossek, U. 2009. *Progressive collapse of structures*. London: Thomas Telford.

Starossek, U., and M. Haberland. 2011. "Approaches to measures of structural robustness." *Struct. Infrastruct. Eng.* 7 (7–8): 625–631. https://doi.org/10.1080/15732479.2010.501562.

Wang, J., W. Wang, and Y. Bao. 2020. "Full-scale test of a steel-concrete composite floor system with moment-resisting connections under a middle-edge column removal scenario." *J. Struct. Eng.* 146 (5): 04020067. https://doi.org/10.1061/(ASCE)ST.1943-541X.0002630.

Wang, J., W. Wang, Y. Bao, and D. Lehman. 2021. "Numerical investigation on progressive collapse resistance of steel-concrete composite floor systems." *Struct. Infrastruct. Eng.* 17 (2): 202–216. https://doi.org/10.1080/15732479.2020.1733622.

Wang, J., W. Wang, D. Lehman, and C. Roeder. 2019a. "Effects of different steel-concrete composite slabs on rigid steel beam-column connection under a column removal scenario." *J. Constr. Steel Res.* 153 (Feb): 55–70. https://doi.org/10.1016/j.jcsr.2018.09.025.

Wang, J., W. Wang, and X. Qian. 2019b. "Progressive collapse simulation of the steel-concrete composite floor system considering ductile fracture of steel." *Eng. Struct.* 200 (Dec): 109701. https://doi.org/10.1016/j.engstruct.2019.109701.

Wang, W., C. Fang, X. Qin, Y. Chen, and L. Li. 2016. "Performance of practical beam-to-SHS column connections against progressive collapse." *Eng. Struct.* 106 (Jan): 332–347. https://doi.org/10.1016/j.engstruct.2015.10.040.

Yang, B., and K. H. Tan. 2013. "Robustness of bolted-angle connections against progressive collapse: Experimental tests of beam-column joints and development of component-based models." *J. Struct. Eng.* 139 (9): 1498–1514. https://doi.org/10.1061/(ASCE)ST.1943-541X.0000749.